FEBS Open Bio 3 (2013) 263–270

FEBS openbio

journal homepage: www.elsevier.com/locate/febsopenbio

Calcium binding by the PKD1 domain regulates interdomain flexibility in *Vibrio cholerae* metalloprotease PrtV☆

Aaron Edwin[a,b], Pramod Rompikuntal[b,c,d], Erik Björn[a], Gunter Stier[a,1], Sun N. Wai[b,c,d], A. Elisabeth Sauer-Eriksson[a,b,*]

[a] Department of Chemistry, Umeå University, Umeå SE-901 87, Sweden
[b] Umeå Centre for Microbial Research (UCMR), Umeå University, Umeå SE-901 87, Sweden
[c] Department of Molecular Biology, Umeå University, Umeå SE-901 87, Sweden
[d] The Laboratory for Molecular Infection Medicine Sweden (MIMS), Umeå University, Umeå SE-901 87, Sweden

ARTICLE INFO

Article history:
Received 12 June 2013
Received in revised form 20 June 2013
Accepted 21 June 2013

Keywords:
Vibrio cholerae
Metalloprotease
PrtV
Polycystic Kidney domains
PKD domain
Atomic resolution
Calcium binding
X-ray crystallography

ABSTRACT

***Vibrio cholerae*, the causative agent of cholera, releases several virulence factors including secreted proteases when it infects its host. These factors attack host cell proteins and break down tissue barriers and cellular matrix components such as collagen, laminin, fibronectin, keratin, elastin, and they induce necrotic tissue damage. The secreted protease PrtV constitutes one virulence factors of *V. cholerae*. It is a metalloprotease belonging to the M6 peptidase family. The protein is expressed as an inactive, multidomain, 102 kDa pre-pro-protein that undergoes several N- and C-terminal modifications after which it is secreted as an intermediate variant of 81 kDa. After secretion from the bacteria, additional proteolytic steps occur to produce the 55 kDa active M6 metalloprotease. The domain arrangement of PrtV is likely to play an important role in these maturation steps, which are known to be regulated by calcium. However, the molecular mechanism by which calcium controls proteolysis is unknown. In this study, we report the atomic resolution crystal structure of the PKD1 domain from *V. cholera* PrtV (residues 755–838) determined at 1.1 Å. The structure reveals a previously uncharacterized Ca^{2+}-binding site located near linker regions between domains. Conformational changes in the Ca^{2+}-free and Ca^{2+}-bound forms suggest that Ca^{2+}-binding at the PKD1 domain controls domain linker flexibility, and plays an important structural role, providing stability to the PrtV protein.**

1. Introduction

The World Health Organization reports 3–5 million cases of cholera every year leading to 100,000–120,000 deaths. The disease is caused by *Vibrio cholerae*, a Gram-negative motile bacterium, which upon infection releases several virulence factors [1]. These include secreted proteases that proteolyze tissue barriers and cellular matrix components, such as collagen, laminin, fibronectin, keratin, elastin and thereby induce necrotic tissue damage [2–4]. Microbial proteases can be classified into four groups on the basis of the essential catalytic residue at their active site. These four groups are: serine proteases, cysteine proteases, aspartate proteases and metalloproteases. Most metalloproteases are zinc-containing proteins [3].

The secreted metalloprotease PrtV constitutes a very potent cytotoxic agent of *V. cholerae* [5,6]. PrtV is cytotoxic for human HCT8 cells. It is also known that the fibrinogen, fibronectin and plasminogen present in human blood plasma can function as substrates for the protease [6]. PrtV belongs to the M6 peptidase family, sharing 37% sequence identity with the Immune Inhibitor A (InhA) from *Bacillus thurengiensis*.

PrtV is expressed as an inactive 102 kDa full-length pre-pro-protein. In addition to a signal peptide, the PrtV protein has four domains: the N-terminal domain (residues 23–105), the M6 domain (residues 106–749), and two Polycystic Kidney Disease domains – PKD1 (residues 755–837) and PKD2 (residues 838–918) (Fig. 1A). The sequence of the N-terminal domain is present in many bacterial proteins; however, its specific function has not yet been identified. The M6 domain constitutes the catalytic metalloprotease domain with the characteristic HexxHxxgxxD Zn^{2+}-binding motif [7]. PKD domains are found in various eukaryotic and prokaryotic proteins; they are relatively short domains of 80–90 amino acids with a characteristic β-sandwich fold [8]. They are usually found in the extracellular parts

[1] Present address: Biochemie-Zentrum der Universität Heidelberg, Im Neuenheimer Feld 328, 69120 Heidelberg, Germany.

* Corresponding author at: Department of Chemistry, Umeå University, Umeå SE-901 87, Sweden. Tel.: +46 90 7865923; fax: +46 90 7865944.
E-mail address: elisabeth.sauer-eriksson@chem.umu.se (A.E. Sauer-Eriksson).

2211-5463/$36.00
http://dx.doi.org/10.1016/j.fob.2013.06.003

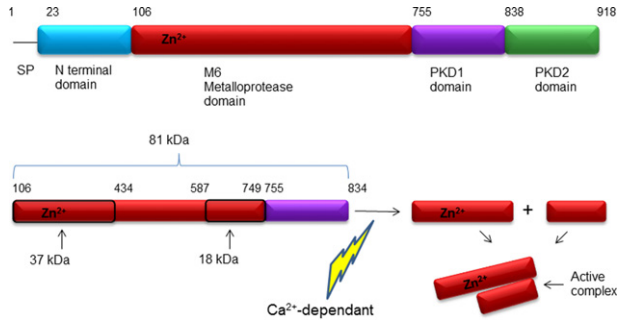

Fig. 1. Domain organization and maturation products of PrtV. (A) A schematic representation of the four domains in 102 kDa full-length PrtV. (B) Ca^{2+}-dependent proteolytic degradation of the 81 kDa pro-protein results in formation of the 55 kDa active complex comprising two chains of 18 and 37 kDa each. Both chains are originally part of the M6 domain. The lightning bolt symbolizes the Ca^{2+}-dependent cleavage between residues Leu749 and Ser750 [6].

of proteins involved in protein–protein or protein–carbohydrate interactions. The function of the PKD domains in PrtV is not fully understood.

To form a catalytically active protease, PrtV undergoes several N- and C-terminal modifications. PrtV is exported from the bacteria as a 81 kDa molecular mass intermediate form that is known to be stabilized by calcium ions [6]. After secretion, this intermediate undergoes further degradation that finally results in the formation of the active 55 kDa M6 metalloprotease form composed of two chains of 18 and 37 kDa (Fig. 1B) [6]. In this study, we present results from a structural study of the PKD1 domain from *V. cholerae* PrtV. The crystal structure, determined at 1.1 Å resolution, revealed a calcium-binding site which stabilizes the 81 kDa form of the protein, and thus plays a regulatory role in its proteolytic activity.

2. Results

2.1. PKD1 cloning, expression and purification

His-ZZ-tagged PKD1 domain from *V. cholerae* was overexpressed in *E. coli* BL21(DE3)pLysS cells and was purified by Ni–NTA agarose chromatography (Edwin et al., manuscript in preparation). The hexahistidine-ZZ fusion tag was cleaved with TEV protease, leaving the PKD1 domain with three extra residues, Gly, Ala and Met at the N-terminus (theoretical molecular mass of the domain is 9.5 kDa). The protein was then purified to homogeneity by size exclusion chromatography. Approximately 15 mg pure protein was obtained from 1 l culture.

2.2. Structure determination

With the X-ray diffraction data from a single crystal, the structure of the 85-residue PKD1 domain (residues Glu755-Asn839) from *V. cholerae* metalloprotease PrtV was determined by the molecular replacement method. The asymmetric unit contained two molecules: chains A and B. Apart from a few residues at the N- and C-termini, all protein residues could be modeled into the electron density. The overall quality of the electron density was excellent with clearly defined hydrogen atoms for most of the residues (Fig. 2). Weak or no electron density was observed for the side-chains of residues Ile757, Lys766, Glu768, Met773, Gln775, Gln830, Lys834 in both chains and residue Thr837 from chain B: these residues are situated at the surface of the molecule. The final model contains residues Ile757-Pro838 of chain A, and residues Ile757-Thr837 of chain B. In both chains, several residues are modeled in multiple conformations (2 or 3). The first two visible residues, Ile757-Ala758, at the N-terminus of chain B are

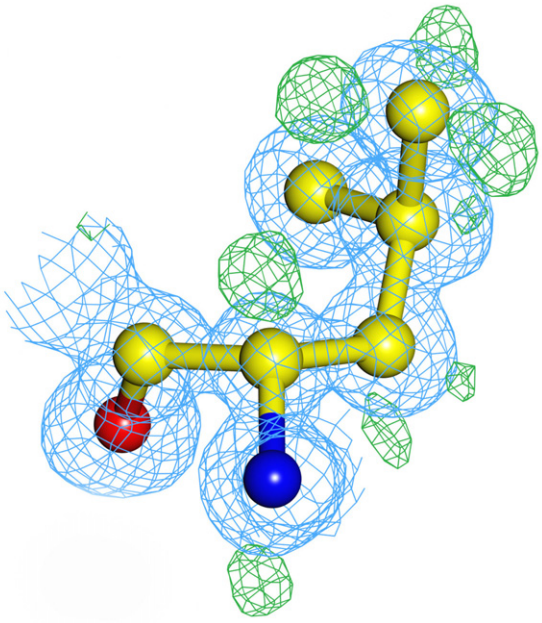

Fig. 2. Difference Fourier maps showing the quality of the electron density at a representative residue (Leu34). The residue is represented as a ball-and-stick model. The *2mFo-DFc* electron density of the refined structure is shown by a blue mesh contoured at 1σ. The green mesh shows the *mFo-DFc* electron density omit map contoured at $+3\sigma$. The positions of hydrogen atoms, not included in refinement or in map calculations, are clearly indicated in the map. (For interpretation of the references to color in this figure legend, the reader is referred to the web version of this article.)

modeled in two conformations depending on whether or not a Ca^{2+} ion is bound to the main chain carbonyl oxygen of Ala758.

300 water molecules, one Ca^{2+} ion, three Na^{+} ions, and three Cl^{-} ions were identified in the structure. One di(hydroxyethyl)ether involved in crystal packing interactions was also identified. Only those water molecules with B-factors below 60 $Å^2$ and forming hydrogen bonds either to protein residues directly or to protein-linked water molecules, were included in the structure. Metal ions were identified on the basis of their geometry, ligand distances, and B-factors. The final *R*-values, $R_{work} = 0.109$ and $R_{free} = 0.140$, are within values expected for structures determined at atomic resolution. Table 1 summarizes the X-ray data collection statistics and refinement of the PKD1 structure. The coordinates and structure factors are deposited in the Protein Data Bank (PDB) (accession code 4L9D).

2.3. The structure of PKD1

As anticipated from sequence analysis, CD measurements, and secondary structure prediction (software Jpred3 [9]), the amino acid chain of the PKD1 domain has an all-β type fold. It comprises two antiparallel β-sheets of three (A, B, E) and four (D, C, F, G) strands, respectively: strands A (A_1: residues Val760-Ala761; A_2: Phe763-Gly769), B (B_1: residues Ser771-Thr777; B_2: Ser779-Asp780) and E (residues Thr804-Tyr807), and strands D (residues Gln796-Thr799), C (residues Val786-Gly793), F (residues Gly811-Asp822), and G (residues Gly824-Asp836). The two β-sheets are packed face-to-face in a β-sandwich – the typical fold for this domain (Fig. 3A) [8]. The core of the β-sandwich is formed by hydrophobic interactions involving residues Pro759, Ala761, Phe763, Leu765, Val772, Ile785, Trp790, Pro803, Trp805, Val815, Leu817, and Val819.

2.4. PKD1 dimerization

Size-exclusion chromatography showed that PKD1 forms dimers at neutral pH. The packing of the molecules in the crystal structure

Table 1
Data collection and refinement statistics.

Data collection	
Beamline	ESRF, ID23–1
Wavelength (Å)	1.0398
Temparature (°C)	−173
Vm (Å^3/Da)	1.46
Space group	$P2_12_12_1$
Number of subunits per asymmetric unit	2
Cell dimesions; *a*, *b*, *c* (Å); α, β, γ (°)	41.80, 50.83, 67.30, 90.0, 90.0, 90.0
Resolution range[a] (Å)	12.0–1.10 (1.15–1.10)
R_{merge} [b] (%)	0.060 (0.175)
$<I/sigI>$	16.7 (7.4)
Completeness for range (%)[a]	99.0 (96.2)
Number of observations	423,614 (45,460)
Number of unique reflections	58,243 (8157)
Refinement	
Resolution range (Å)	12.0–1.1 (1.13–1.10)
R-work[c]	0.109 (0.139)
R-free[d]	0.140 (0.180)
Number of atoms	1747
Protein	1433
Ligands	14
Waters	300
RMSD bond length (Å)	0.020
RMSD bond angle (°)	2.192
Average B	
Protein atoms (Å^2)	8.8
Ca^{2+} (Å^2)	13.8
PEG (Å^2)	21.3
Other ligands (Å^2)	12.3
Water molecules (Å^2)	21.7
Ramachandran plot	
Allowed region (%)	98.7
Number of outliers	0

[a] The numbers in parentheses refer to the highest resolution bin.
[b] R_{merge} for replicate reflections, $R = \Sigma\,|I_{hi} - <I_h>|/\Sigma|<I_h>|$; I_{hi} = intensity measured for reflection *h* in data set *i*, $<I_h>$ = average intensity for reflection *h* calculated from replicate data.
[c] *R*-factor = $\Sigma||F_o| - |F_c||/\Sigma|F_o|$; F_o and F_c are the observed and calculated structure factors, respectively.
[d] R_{free} based upon 5% of the data randomly culled and not used in the refinement.

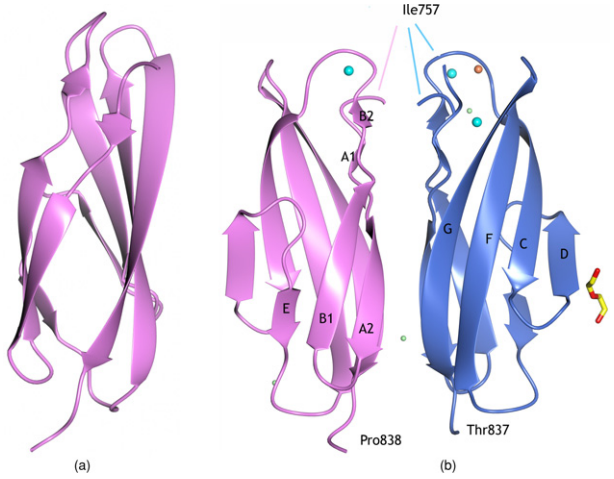

Fig. 3. Ribbon representation of the PKD1 domain structure shown in two orientations. (A) The β-sandwich structure of the PDK1 domain is divided into two sheets of three and four β-strands each. (B) Two molecules (Interface-I) were present in the asymmetric unit, which could represent the dimer seen in solution. Sodium, chloride and calcium ions are colored in cyan, light green and orange, respectively. The di(hydroxyethyl)ether is shown as a stick. The N-terminal end of monomer B (blue ribbon) has two conformations as indicated by the two blue lines. (For interpretation of the references to color in this figure legend, the reader is referred to the web version of this article.)

also indicated that PKD1 is dimeric. The asymmetric unit comprises two molecules of PKD1, monomers A and B, and crystal packing contacts provided two alternative possibilities for homodimeric PKD1 packing interactions. At the first dimer interface, monomers A and B are packed head-to-head to form a four-β-strand arrangement comprising symmetry-related A and G strands (Fig. 3B). Across from the interface, charged side chains of A- and B-Arg762 residues and B- and A-Asp827 residues form two symmetry-related salt-bridges. Other contacts involve the Nε1 atoms of A- and B-His829, which form hydrogen bonds via a bridging water molecule to the Oε2 atom of B- and A-Glu764, respectively. A high-occupancy chloride ion bound to symmetry-related amide groups of A- and B-Lys834 and to three water molecules was identified at this interface. Furthermore, A- and B-Gln831 form hydrogen bonds to the main-chain amido group of B- and A-Leu705; however, the glutamate side chains are flexible and are therefore modeled in two different conformations. The interface, which we refer to as Interface-I, is predominantly polar, with more than 50 water molecules associated with it. A few hydrophobic contacts exist between symmetry-related residues A- and B-Val760, and the hydrophobic part of the A- and B-Arg762 residues.

The second putative dimer interface, Interface-II, is formed between two symmetry-related A- and B-β-sheets, D-C-F-G. The monomers are packed head-to-tail and contacts are primarily formed between threonine and aspartate side chains, mediated by bridging water molecules. Interestingly, the only direct side-chain to side-chain contact at this interface is between two symmetry-related A- and B-Asp791 residues (the distance between their Oδ2 atoms is 2.5 Å).

PISA is an interactive tool for exploration of protein interfaces [10]. PISA analysis of the two interfaces identified in the PKD1 crystals suggested that only Interface-I would be stable in solution. The solvation energy effect, Δ^iG, of this interface was calculated to be −64.6 kcal/mol. Furthermore, ΔG^{diss}, which indicates the free energy of assembly dissociation, was calculated to be 7.3 kcal/mol. Δ^iG and ΔG^{diss} for Interface-II was calculated as −58.5 and −1.8 kcal/mol, respectively. The size of buried area was estimated to be 2330 and 2300 Å^2 for Interface-I and -II, respectively. Taken together, the output data from PISA indicated that only the dimer Interface-I (as shown in Fig. 1B) constitutes a stable interface.

2.5. Ca^{2+}-binding site in PKD1

The high quality of the electron density maps allowed the unambiguous identification of a Ca^{2+}-binding site in monomer B of PKD1. The site is located at one end of the β-sandwich structure near the N-terminal residues of the PKD1 domain. The site is formed by two loops, connecting β-strand B with C, and β-strand F with G. In addition, the first residues of β-strand A1, positioned at the N-terminal end of the PKD1 domain, are involved in Ca^{2+}-binding. The occupancy of the Ca^{2+} ion was refined to 0.5 (i.e., 50% occupancy in the crystal), and its presence was deduced from the geometry, ligand distances, and B-factors. The Ca^{2+} ion binds to four carboxylate atoms from a conserved acidic motif and to one water molecule (Fig. 4A and B). The coordination sphere of the five-ligand-coordinated Ca^{2+} ion is irregular (Findgeo server [11]). This is not uncommon as calcium-binding sites in proteins in general are highly irregular with large variation in ligand type, length, and angle of the metal coordination shell [12].

To further investigate the Ca^{2+}-binding properties of the protein, we analyzed pure protein samples after size-exclusion chromatography for the presence of metal ions using optical emission spectrometry. The analysis was performed both on purified protein samples without added metals, and on samples to which we added Ca^{2+}-ions or Mg^{2+}-ions. Excess, unbound metals were removed from the protein solution by extensive dialysis overnight. We found that Ca^{2+}-ions bound in a 1:1 ratio to the PKD1 protein in solution even without the addition of Ca^{2+}-ions. Furthermore, the analysis also showed that

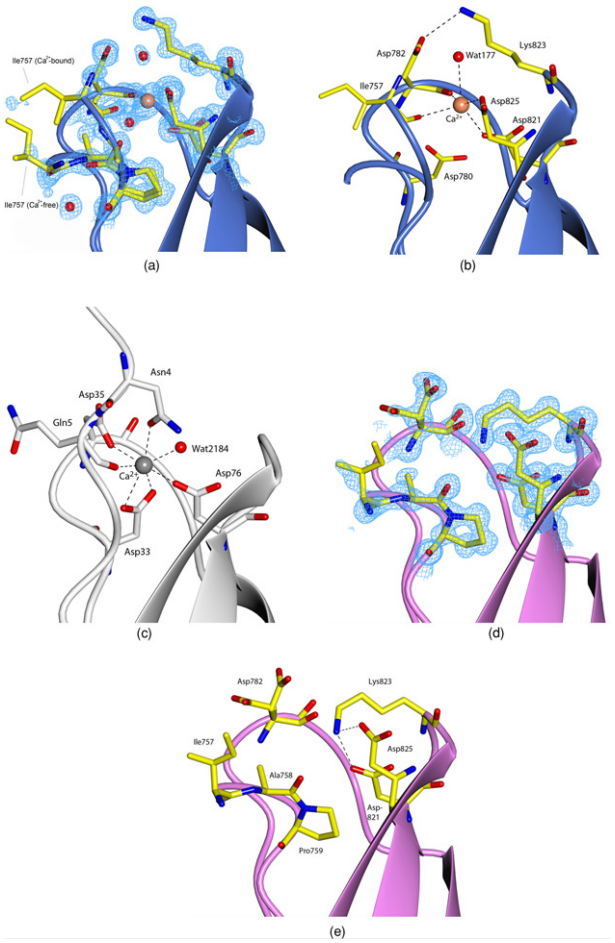

Fig. 4. Calcium-binding site in the PKD1 domain. (A) One calcium-binding site was identified in monomer B and refined at 50% occupancy. (B) The same figure as in (A) but without electron density, and with hydrogen and metal bonds indicated as dotted lines. (C) The calcium-binding site in the PKD domain from glycoside hydrolase CtCel9D from *Clostridium thermocellum* (pdb code 2C4X). (D) The calcium-free conformation in monomer A of PKD1. In particular, Lys823 has a different orientation in the calcium-bound and calcium-free states. (E) The same figure as in (D) with hydrogen bonds indicated. The *2mFo-DFc* electron density of the refined structure is shown in panels (A) and (D) by a blue mesh contoured at 1σ. (For interpretation of the references to color in this figure legend, the reader is referred to the web version of this article.)

the Ca^{2+}-ions could not be substituted by Mg^{2+}-ions.

Structural similarity searches using the DALI server [13,14] identified a number of structures similar to PKD1. The top 6 DALI hits are presented in Table 2. Generally, the protein structures identified by DALI comprised other PKD domains. Analysis of the top DALI hits showed that Ca^{2+}-binding has been previously observed in at least one of them — the C-terminal PKD domain of the glycoside hydrolase CtCel9D from *Clostridium thermocellum* (pdb code 2C4X) [15]. Structural comparisons showed the topology of the Ca^{2+}-binding site of PKD1 and that of PDB ID:2C4X to be very similar, even though the ligand-binding partners are not identical (Table 3 and, Fig. 4B and C).

The refined Ca^{2+}-ion in monomer B showed about 50% occupancy. Furthermore, the N-terminal residues, Ile757 and Ala758, were refined in two conformations with 50% occupancy each. In one of these conformations, the main chain carbonyl oxygen of Ala758 constitutes one of the Ca^{2+}-binding ligands, extending the β-strand A1 by one residue, in agreement with what is observed in the 2C4X structure. In the second conformation, the carbonyl oxygen of Ala758 has a different orientation. The main chain of the first two N-terminal residues has changed its direction approximately 90°, with respect to its conformation in the Ca^{2+}-bound form (Fig. 4A and B). We refer to this

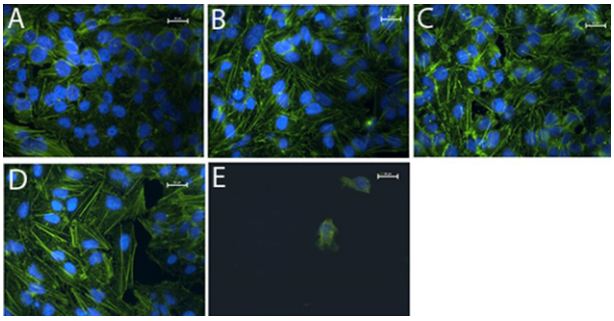

Fig. 5. HCT8 cells after 6 h of incubation with pure PKD1 domain at (A) 20 nM, (B) 50 nM and (C) 200 nM concentration. No effects on cell morphology were observed after incubation with PKD1 even at high concentrations. (D) shows control HCT8 cells, and (E) shows the cytotoxic effect on HCT8 cells after incubation with 20 nM of PrtV purified in the 55 kDa active form [6]. Actin filaments and nuclei were stained with phalloidin (green color) and DAPI (blue color), respectively. (For interpretation of the references to color in this figure legend, the reader is referred to the web version of this article.)

conformation of the N-terminal residues as the Ca^{2+}-free form of the PKD1 domain. In the calcium-free monomer A, the N-terminal residues occupy positions assigned with the Ca^{2+}-free conformation (Fig. 4D and E). Lys823 and Asp825, both positioned at the FG-loop, have side-chain rotamers such that the Nε atom of Lys823 is positioned right at the binding site for the Ca^{2+}-ion. No water molecules bound in the Ca^{2+}-binding site of the Ca^{2+}-free monomer A.

2.6. The PKD1 domain is not toxic for HCT8 cells

To investigate if the PKD1 domain of PrtV protein is cytotoxic in mammalian cells, we incubated the human colon carcinoma (HCT8) cells with different concentrations of purified PKD1 protein as described in Materials and methods. No significant morphological changes of HCT8 cells were observed when the cells were incubated with the purified PKD1 domain, although purified extracellular 81 kDa PrtV pro-protein showed a cytotoxic effect leading to cell death (Fig. 5).

2.7. Calcium binding provides interdomain stability to PrtV in vivo

It is known that calcium ions stabilize the 81 kDa pro-protein *in vitro* [6]. To test the effect *in vivo*, *V. cholera* strain KAS202 overexpressing full length native PrtV were grown in minimal media containing high (5 mM) and low (20 μM) concentrations of Ca^{2+} ions. To verify expression of the PrtV protein at the low calcium concentration, we performed the experiment in the same *V. cholera* strain lacking the haemagglutinin protease HapA and two of its regulatory proteins: leucine aminopeptidase and leucine aminopeptidase X [6]. HapA constitutes the major extracellular protease in *V. cholera*, and its expression is regulated by the HapR regulon [21]. All cultures grow equally well at the two calcium concentrations (results not shown). Filtered supernatant of the cell cultures was separated on a SDS PAGE and the presence of secreted PrtV fragments was detected with polyclonal antibodies against PrtV (Fig. 6). Our results show that the integrity of the secreted 81 kDa PrtV pro-fragment *in vivo* is dependent on the presence of calcium ion, and, as shown previously, protease(s) regulated by the HapR-pathway are involved in degradation of PrtV fragments [6].

3. Discussion

The secreted metalloprotease PrtV from *V. cholerae* was recently identified as a potent virulence agent during infection of human HCT8 cells [5]. For proper function, the 102 kDa PrtV must first be degraded

Table 2
DALI top ranking structures.

Protein	Chain	PDB code	Z-score	rmsd	Alignment length	% seq. id	Ca^{2+} bind-ing	Reference
PKD, collagenase	A	2Y72	13.3	1.2	81	41	No	[16]
PKD, endoglucanase	A	2C4X	12.8	1.5	82	39	Yes	[15]
PKD, surface layer protein	A	1L0Q	12.0	1.7	77	32	No	[17]
Neural cell adhesion Molecule 1	D	1LWR	9.8	2.1	82	15	No	[18]
Neural Cell Adhesion Molecule 2	A	2XYC	9.2	2.2	80	11	No	[19]
Fragment fibronectin	A	3T1W	9.0	2.3	79	9	No	[20]

Table 3
Ca^{2+} binding geometries.

PKD1 domain (this work)			2C4X [15]		
Metal	Ligand	Distance (Å)	Metal	Ligand	Distance (Å)
Ca^{2+}	O Asp782	2.36	Ca^{2+}	Oδ1 Asp35	2.35
Ca^{2+}	Oδ2 Asp821	2.48	Ca^{2+}	Oδ2 Asp76	2.44
Ca^{2+}	O Ile757	2.48	Ca^{2+}	O Gln5	2.40
Ca^{2+}	O Wat177	2.83	Ca^{2+}	O Wat 2184	2.42
Ca^{2+}	Oδ2 Asp825	2.46	Ca^{2+}	Ala80	Not binding
Ca^{2+}	Oδ1 Asp780	Not binding (4.01)	Ca^{2+}	Oδ1 Asp33	2.50
Ca^{2+}	Oδ1 Asp780	Not binding (4.32)	Ca^{2+}	Oδ2 Asp33	2.36
Ca^{2+}	Asn756	Not in construct	Ca^{2+}	Oδ1 Asn4	2.40

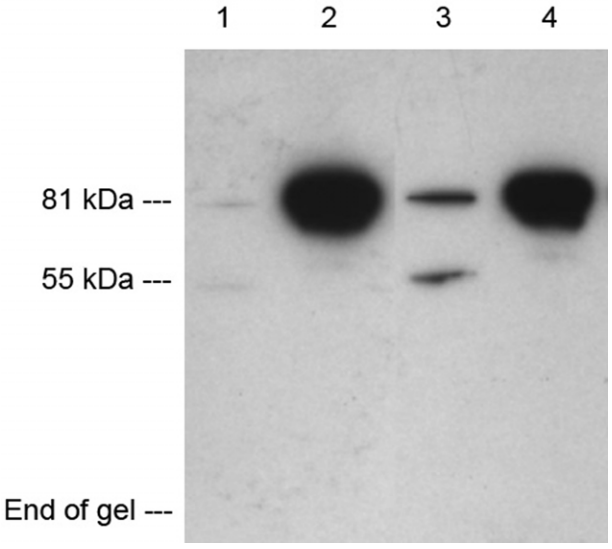

Fig. 6. Immunoblot of PrtV protein secreted from *V. cholerae* strain KAS202 (ΔprtV) (lane 1 and 2) and KAS202 (Δlap ΔlapX ΔhapA, ΔprtV) (lane 3 and 4). Both strains carried a plasmid pKVA232 overexpressing native PrtV at two different concentrations of calcium ions: 20 μM (lane 1 and 3) or 5 mM (lane 2 and 4). At high concentrations of calcium the secreted 81 kDa pro-fragment of PrtV is protected from degradation (lane 2 and 4). At low calcium concentration however the PrtV pro-fragment is secreted (lane 3) but completely degraded (lane 1). Complete degradation of secreted PrtV did not occur in the Δlap ΔlapX ΔhapA deletion mutant (lane 3). This verifies that protease(s), regulated by the HapR-pathway, can degrade PrtV fragment (compare lane 1 and lane 3) [5].

and then secreted by the bacteria as an 81 kDa intermediate form. Once outside the cell, the pro-protein undergoes several additional modifications steps, which finally results in the active 55 kDa M6 metalloprotease form, comprising the heterodimer of two chains of 18 and 37 kDa each, Fig. 1 [5].

PrtV comprises two PKD domains and, in this work, the structure of one of them — the 87 residue PKD1 domain – was determined at atomic resolution. The PKD domain name is derived from the *pkd1* gene, which is mutated in autosomal-dominant Polycystic Kidney Disease. The product of this gene harbors sixteen copies of this domain in the extracellular part of polycystin-1, a cell surface glycoprotein [8,22,23]. PKD domains from different proteins and organisms share low sequence identity but are structurally similar. Interestingly, they serve different functions even though most of them are found in the extracellular parts of larger protein adhesins where they are involved in protein–protein or protein–carbohydrate interactions. For polycystin-1, the PKD domains are involved in intermolecular interactions, where they play an important role in intercellular adhesion [24]. The PKD domain of the serine protease ColG from *Pseudoalteromonas* sp. *SM9913* binds to collagen and allows swelling of the target leading to a more efficient proteolysis [25]. As a further example, binding of the PKD domain to chitin is necessary for chitin degradation by chitinase A from the marine bacterium, *Pseudoalteromonas piscicida* [26]. It is likely that the PKD domains present in *V. cholerae* PrtV also are involved in intermolecular interactions.

We expressed the PKD1 domain in *E. coli* and purified the protein to homogeneity. The 3D-structure was solved by the molecular replacement methods at 1.1 Å resolution. The protein folds into an all-β type structure of 2 β-sheets typical for PKD domains (Fig. 3). Purified PKD1 domains are dimeric in solution and two plausible interfaces were also identified in the crystalline form. Analysis of the two interfaces suggests that Interface-I is more likely than Interface-II to constitute the dimer observed in solution. The second Interface-II involves predominantly one, close side-chain to side-chain contact between two symmetry-related aspartic acids; these contacts could explain why crystals only could be obtained at low pH (pH 5–5.5). The biological relevance, if any, of the dimer form of PKD1 remains to be elucidated. However, purified PKD1 domains are not toxic for human HTC8 cells (Fig. 5).

The secreted and purified 81 kDa pro-protein is known to be stabilized by calcium ions [6]. In the crystal structure of the PKD1 domain, a Ca^{2+}-binding site in at the N-terminal region of the domain was identified (Fig. 4A). Multiple lines of evidence suggest that the PKD1-bound Ca^{2+}-ion constitutes a natural ligand for the PrtV protein *in vivo*. First, the Ca^{2+}-binding site that we identified is not unique for the PrtV PKD1 domain – nearly identical binding sites have been identified in other PKD domains e.g., microbial cellulases [15]. Second, our metal content analysis verified that Ca^{2+} ions bind to the purified PKD1 domain in solution at a 1:1 ratio. Ca^{2+} ions occupy only one of the two monomers present in the asymmetric unit and at 50% occupancy. Presumably, the 1.2 M sodium citrate that is part

of the crystallization conditions chelates the calcium from the protein solution however the crystal packing interaction favors only the completely Ca^{2+}-free conformation at monomer A. The 1.1 Å structure presented here was determined with 10 mM $CaCl_2$ present in the crystallization conditions. Increasing Ca^{2+}-ion concentration in the crystallization conditions did not affect the structure. We determined a 1.6 Å structure of the PKD1 domain in the presence of 150 mM $CaCl_2$. This structure displayed no structural changes compared to the 1.1 Å structure, nor did the occupancy of the Ca^{2+} ion in monomer B change significantly (data not shown). So far we have not succeeded in determining the structure of the complete apo-form of the PKD1 domain. When all Ca^{2+} ions were removed from the protein by extensive dialysis in the presence of 1 mM EDTA, no crystals could be obtained in the subsequent crystallization trials. Furthermore, back-soaking Ca^{2+}-containing crystals in a calcium-free crystallization solution containing EDTA also rendered the crystals unsuitable for diffraction studies. Fortunately, in-depth information about Ca^{2+}-induced conformational changes in the PKD1 domain could be obtained by comparing the structures of the Ca^{2+}-free A monomer with the Ca^{2+}-bound B monomer. The structural analysis showed that calcium binding causes large conformational changes in the N-terminal half of the PKD1 domain (Fig. 4).

The calcium-dependent stability of PrtV was tested *in vivo*. The resting concentration of Ca^{2+} in the cytoplasm is normally maintained in the range of 10–100 nM, whereas the concentration is in the mM range outside the cell [27]. *V. cholera* overexpressing the native PrtV protein were grown in minimal media supplemented with either low (20 μM) or high (5 mM) concentrations of calcium ions. Presence of PrtV in the media was investigated directly with immunoblot analysis. The results, shown in Fig. 6, showed that PrtV secreted by the bacteria into the media with low, 20 μM, calcium concentration will rapidly be degraded into low molecular weight fragments not detectable on the immunoblot. This complete degradation of the protein is due to secreted proteases present in the media. Purified 81 kDa PrtV degrades into two interacting poly-peptide chains of 37 and 18 kDa in the absence of calcium ions [6]. Most likely this maturation process of the pro-protein takes place inside the host cell. A similar maturation is described for other metalloproteases including the immune inhibitor A from *Bacillus cereus* and *B. anthracis* [28,29].

One of the proteolytic cleavage sites on the 81 kDa pro-protein has been identified as a short, 5-residue linker that connects the C-terminal end of the M6 domain with the N-terminal end of the PKD1 domain (Fig. 7A) [6]. This site is positioned only 3 residues upstream from the calcium-binding site in PKD1. We therefore hypothesize that PKD1-bound Ca^{2+} ions stabilize the 81 kDa pro-protein outside the bacterial cell, and protect it from degradation. In our current model, the N-terminal residues of the PKD1 domain are locked by bound Ca^{2+} ions in an extended β-strand conformation that protects the 5-residue linker (which connects the M6 and PKD1 domains) from proteolysis. If the PKD1 domain is depleted of Ca^{2+} ions, conformational changes of the N-terminal residues expose the 5-residue linker to proteolysis (Fig. 7B).

On the basis of sequence analysis, it seems possible that the PKD2 domain of PrtV could bind calcium as well (Fig. 8). Thus, the protease binds calcium ions in the vicinity of two regions involved in the proteolytic maturation process. The PKD2 domain, however, is not secreted from the cell (Fig. 1B). The structure of the M6 domain is currently unknown, and it remains to be seen if calcium-binding to this domain is involved in the maturation process of the protein as well.

4. Experimental procedure

4.1. Protein expression and purification

The cloning, overexpression and purification of the PKD1 domain (residues 755–839) will be described separately (Edwin et al., manuscript in preparation). Briefly, the PKD1 domain was cloned into the pETZZ1a vector [30] and overexpressed in *E. coli* Bl21 (DE3) pLysS (Novagen) cells. The protein was purified on a Ni-NTA agarose (Qiagen) column followed by a Superdex 200–16/60 size exclusion column (GE Healthcare). During purification, the 6-His ZZ-tag was removed with tobacco etch virus (TEV) protease, leaving three extra residues Gly, Ala and Met at the N-terminus of the domain. Pure fractions of the protein in 20 mM Tris pH 8.0 and 150 mM NaCl (buffer A) were pooled and concentrated to 20 mg ml^{-1} (2.1 μM) and stored at −80 °C.

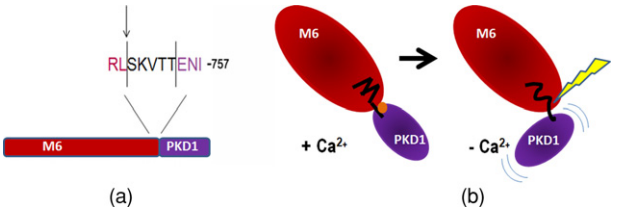

Fig. 7. Suggested mechanism for calcium-dependent stabilization of PrtV. (A) The cleavage site after residue Leu749 (marked with an arrow) is connected with a 5-residue linker to the PKD1 domain. (B) *Left panel:* Ca^{2+} (orange sphere) bound at the N-terminal end of the PKD1 domain shields the accessibility of the neighboring residues. *Right panel:* In the Ca^{2+}-free form, the orientation of the N-terminal β-strand A1 changes, which makes the cleavage site at residue Leu749 accessible for proteolysis. The site of proteolysis is indicated with a yellow arrow. (For interpretation of the references to color in this figure legend, the reader is referred to the web version of this article.)

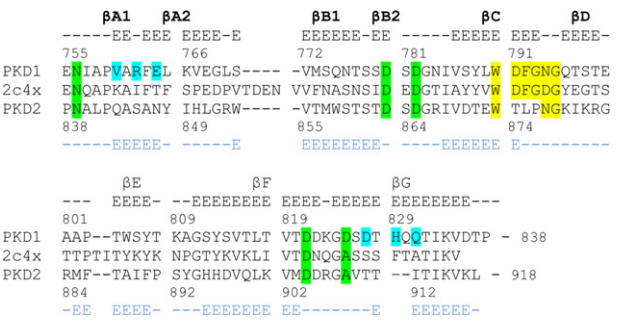

Fig. 8. Sequence alignment (Blast, [39]) of PKD1 and PKD2 domains from *V. cholerae* PrtV, and the PKD domain of the glycoside hydrolase CtCel9D from *Clostridium thermocellum* (pdb code 2C4X, [15]). The sequence identity is 39% between the PKD1 and PKD2 domains, and 40% between the PKD1 and the PKD domain present in the 2C4X structure. The domain border between PKD1 and PKD2 is not well defined. Secondary structural elements from the current structure of PKD1 are shown in black (E, β-strands). Residues part of Interface-I are boxed in cyan, while residues found to be important for calcium binding, are boxed in green. The secondary structure elements predicted for PKD2 with Jpred3 [9] are shown in blue (E, β-strands). Interestingly, the WDFGDG sequence marked in yellow that is generally highly conserved in PKD domains [8] is not conserved in the PKD2 domain. (For interpretation of the references to color in this figure legend, the reader is referred to the web version of this article.)

4.2. Analysis of biological activity of PKD1 domain

HCT8 cells were seeded in 24-well plates (Thermo Scientific Nunclon) and grown to 50% confluence [31]. Purified PKD1 protein (50 μl, 20–200 nM) was added to the cells. Cytotoxic effects in the form of cell rounding and detachment were compared with the responses of control cells for up to 6 h. Cells were fixed with 2% paraformaldehyde in phosphate-buffered saline (PBS, pH 7.3, Sigma–Aldrich) for 10 minutes. After fixation, cells were washed twice with PBS and incubated with 0.1 M glycine for 5 min at room temperature. After washing twice with PBS, the cells were permeabilized with 0.5% Triton X-100 (Sigma–Aldrich). Actin filaments were stained using Alexa Fluor 488 phalloidin (Molecular Probes, Invitrogen) containing 1% bovine serum albumin (BSA) (Sigma–Aldrich). After thorough washing with PBS,

the nuclei were stained (1:5000) for 5 min with 4′,6-diamidino-2-phenylindole dihydrochloride, DAPI, (Sigma–Aldrich) before mounting in a fluorescent mounting medium (Daco Co.). Cells were analyzed using a NIKON Eclipse 90i microscope, and photographed with a Himamatsu BW digital camera (12 bit) (Hamamatsu, Japan).

4.3. PrtV stability assay

Singles colonies of *V. cholerae* strains KAS202 (ΔprtV) and KAS202 (Δlap ΔlapX ΔhapA, ΔprtV), both carrying a plasmid pKVA232 overexpressing native PrtV under the control of an arabinose-inducible promotor [6], were inoculated in 5 ml Luria Bertani medium containing 1% glucose and 50 μg/ml carbenicillin. The pre-cultures were grown with aeration for ∼12 h (overnight) at 37 °C. Subcultures at a 1:100 dilution were started by inoculating 0.5 ml into 50 ml of 25 mM Tris–buffered media pH 7.4 supplemented with 0.1% casamino acids, 50 μg/ml tryptophan, 150 mM NaCl, 30 mM KCl, 20 mM $(NH_4)_2SO_4$, 1 mM $MgSO_4$, 2 mM KH_2PO_4 0.5% glucose, 50 μg/ml carbenicillin and trace elements (50 μM $FeCl_3$, 20 μM $CaCl_2$, 10 μM $MnCl_2$, 10 μM $ZnSO_4$, 2 μM $CoCl_2$, 2 μM $CuCl_2$, 2 μM $NiCl_2$, 2 μM Na_2MoO_4, and 2 μM H_3BO_3). Cells were grown in either low, 20 μM, or high, 5 mM, calcium concentrations. At $OD_{600} = 0.6$, protein expression was induced by adding 0.002% w/v arabinose. After growing for 12 h at 30 °C, 5 μl of filtered supernatant was mixed with an equal volume of SDS–PAGE loading buffer. The sample was boiled for 5 min and analyzed on a 10% SDS–PAGE and then blotted onto a PVDF membrane. Immunological detection was performed using polyclonal rabbit anti PrtV antibodies [5]. Anti-rabbit horseradish peroxidase-conjugate was used as a secondary antiserum at a final dilution of 1:20,000. The ECL$^+$ chemiluminescence system was used to detect the level of chemiluminescence that was then monitored using a Flour-S MultiImager (BioRad) and by autoradiography.

4.4. Metal content analysis

PKD1 samples, with and without added calcium or magnesium ions, were tested for their metal content. The final protein concentration was 50 nM in buffer A. Metal ions ($MgCl_2$ and $CaCl_2$) were added at a final concentration of 5 mM and incubated for 2 h. All samples (including the controls without added Ca^{2+}) were extensively dialyzed against buffer A to ensure complete removal of unbound calcium from the solution. The samples were diluted five times and concentrations of calcium and magnesium determined by inductively-coupled plasma-optical emission spectrometry (PerkinElmer Optima 2000DV). An external calibration and axial viewing mode at wavelengths 315.887 and 317.933 nm were used for calcium and 279.077 and 285.213 nm for magnesium.

4.5. Crystallization, X-ray diffraction data collection, and structural refinement

Initial screening for crystallization conditions was done with the reservoir solutions from Crystal Screen and Crystal Screen 2 (Hampton Research) and the sitting-drop vapor-diffusion method. The protein concentration was 20 mg/ml in buffer A. Equal volumes (100 nl) of protein and reservoir solutions were placed in 96 well plates (Innovadyne Technologies Inc.) using a nanodrop pipetting robot (Mosquito, TTP Labtech). Crystallization hits were optimized using the hanging-drop vapor diffusion method in XRL plates (Molecular Dimensions). The PKD1 domain was crystallized in an equal volume (2 + 2 μl) of protein (20 mg/ml) and well solution. The best diffracting crystals grew in 1.2 M sodium citrate, pH 5.5, and 20% (w/v) PEG 8K at 18°C to dimensions 0.2 × 0.2 × 0.3 mm^3 within 2 days.

Diffraction data from a single crystal were recorded at −173 °C at beam line ID23–1 at the European Synchrotron Radiation Facility (ESRF), in Grenoble, France. A total of 360 frames of data with an oscillation angle of 0.5° was collected at a wavelength of 1.0398 Å. The data set was processed with XDS [32] and scaled using SCALA from the CCP4 software suite [33]. The space group was $P2_12_12_1$ with two subunits per asymmetric unit. The PKD1 structure was solved using AUTO-RICKSHAW: the EMBL-Hamburg automated crystal structure determination platform [34,35]. The input diffraction data were converted for use in AUTO-RICKSHAW with software from CCP4 [33]. The structure was solved by molecular replacement, and the Arp/wARP module for tracing secondary structure in AUTO-RICKSHAW correctly built 81 of the 87 amino acid in the protein. Manual map inspection and model building were performed with COOT [36,37] and positional refinement with REFMAC5 [33], using the maximum likelihood residual, anisotropic scaling, bulk-solvent correction and atomic displacement parameter refinement [38]. 5% of the observed structure factors were not included in the refinement so that they could be used for the free *R*-factor calculations. Throughout the refinement, the protein subunits were treated independently. Water molecules, double conformations, and solvent molecules were built from scratch into the electron density (mF_o-DF_c and $2mF_o$-DF_c) maps. The resolution limit was subsequently increased to 1.1 Å to ensure stable refinement. Toward the end of the refinement, individual anisotropic B factors were refined for all atoms. For residues whose side-chains were observed in discrete alternate conformations, the occupancy of each conformation was manually estimated (sum of occupancies = 1). The occupancies of some metal ions were less than 1. In the final stages, hydrogen atoms were added in riding-model positions during refinement. Molecular graphics were produced using CCP4mg [33]. Homology searches were performed with DALI [13,14].

Database

The structure factor file and the atomic coordinates of the PKD1 domain of *Vibrio cholerae* metalloprotease PrtV have been deposited in the Protein Data Bank under the accession number 4L9D.

Acknowledgements

We thank the European Synchrotron Radiation Facility (Grenoble, France) for provision of synchrotron radiation facilities, and Drs. Karina Persson, Uwe H. Sauer, and Tobias Hainzl for valuable ideas and discussions; Jagan Mohan, Christin Grundström, and Mitesh Dongre for technical assistance, and Terese Bergfors, Uppsala University, for critical reading of the manuscript. The work was performed at the Umeå Centre for Microbial Research (UCMR) and was further supported by the Kempe Foundation and the Swedish Research Council; project K2013-67X-13001-15-3.

References

[1] Harris, J.B., LaRocque, R.C., Qadri, F., Ryan, E.T. and Calderwood, S.B. (2012) Cholera. Lancet 379, 2466–2476.
[2] Miyoshi, S. and Shinoda, S. (2000) Microbial metalloproteases and pathogenesis. Microbes Infect. 2, 91–98.
[3] Hase, C.C. and Finkelstein, R.A. (1993) Bacterial extracellular zinc-containing metalloproteases. Microbiol. Rev. 57, 823–837.
[4] Shinoda, S. and Miyoshi, S. (2011) Proteases produced by vibrios. Biocontrol Sci. 16, 1–11.
[5] Vaitkevicius, K., Lindmark, B., Ou, G., Song, T., Toma, C., Iwanaga, M. et al. (2006) A *Vibrio cholerae* protease needed for killing of *Caenorhabditis elegans* has a role in protection from natural predator grazing. Proc. Natl. Acad. Sci. USA 103, 9280–9285.
[6] Vaitkevicius, K., Rompikuntal, P.K., Lindmark, B., Vaitkevicius, R., Song, T. and Wai, S.N. (2008) The metalloprotease PrtV from *Vibrio cholerae*. FEBS J. 275, 3167–3177.
[7] Kurisu, G., Kinoshita, T., Sugimoto, A., Nagara, A., Kai, Y., Kasai, N. et al. (1997) Structure of the zinc endoprotease from *Streptomyces caespitosus*. J. Biochem. 121, 304–308.
[8] Bycroft, M., Bateman, A., Clarke, J., Hamill, S.J., Sandford, R., Thomas, R.L. et al. (1999) The structure of a PKD domain from polycystin-1: implications for polycystic kidney disease. EMBO J. 18, 297–305.

[9] Cole, C., Barber, J.D. and Barton, G.J. (2008) The Jpred 3 secondary structure prediction server. Nucleic Acids Res. 36, W197–W201.
[10] Krissinel, E. and Henrick, K. (2007) Inference of macromolecular assemblies from crystalline state. J. Mol. Biol. 372, 774–797.
[11] Andreini, C., Cavallaro, G. and Lorenzini, S. (2012) FindGeo: a tool for determining metal coordination geometry. Bioinformatics 28, 1658–1660.
[12] Yang, W., Lee, H.W., Hellinga, H. and Yang, J.J. (2002) Structural analysis, identification, and design of calcium-binding sites in proteins. Proteins 47, 344–356.
[13] Holm, L. and Sander, C. (1993) Protein structure comparison by alignment of distance matrices. J. Mol. Biol. 233, 123–138.
[14] Holm, L., Kaariainen, S., Rosenstrom, P. and Schenkel, A. (2008) Searching protein structure databases with DaliLite v.3. Bioinformatics 24, 2780–2781.
[15] Najmudin, S., Guerreiro, C.I., Carvalho, A.L., Prates, J.A., Correia, M.A., Alves, V.D. et al. (2006) Xyloglucan is recognized by carbohydrate-binding modules that interact with beta-glucan chains. J. Biol. Chem. 281, 8815–8828.
[16] Eckhard, U., Schonauer, E., Nuss, D. and Brandstetter, H. (2011) Structure of collagenase G reveals a chew-and-digest mechanism of bacterial collagenolysis. Nat. Struct. Mol. Biol. 18, 1109–1114.
[17] Jing, H., Takagi, J., Liu, J.H., Lindgren, S., Zhang, R.G., Joachimiak, A. et al. (2002) Archaeal surface layer proteins contain beta propeller, PKD, and beta helix domains and are related to metazoan cell surface proteins. Structure 10, 1453–1464.
[18] Kiselyov, V.V., Skladchikova, G., Hinsby, A.M., Jensen, P.H., Kulahin, N., Soroka, V. et al. (2003) Structural basis for a direct interaction between FGFR1 and NCAM and evidence for a regulatory role of ATP. Structure 11, 691–701.
[19] Kulahin, N., Kristensen, O., Rasmussen, K.K., Olsen, L., Rydberg, P., Vestergaard, B. et al. (2011) Structural model and trans-interaction of the entire ectodomain of the olfactory cell adhesion molecule. Structure 19, 203–211.
[20] Schiefner, A., Gebauer, M. and Skerra, A. (2012) Extra-domain B in oncofetal fibronectin structurally promotes fibrillar head-to-tail dimerization of extracellular matrix protein. J. Biol. Chem. 287, 17578–17588.
[21] Benitez, J.A., Silva, A.J. and Finkelstein, R.A. (2001) Environmental signals controlling production of hemagglutinin/protease in *Vibrio cholerae*. Infect. Immun. 69, 6549–6553.
[22] Consortium, T.I.P.K.D. (1995) Polycystic kidney disease: the complete structure of the PKD1 gene and its protein. The International Polycystic Kidney Disease Consortium. Cell 81, 289–298.
[23] Hughes, J., Ward, C.J., Peral, B., Aspinwall, R., Clark, K., San Millan, J.L. et al. (1995) The polycystic kidney disease 1 (PKD1) gene encodes a novel protein with multiple cell recognition domains. Nat. Genet. 10, 151–160.
[24] Ibraghimov-Beskrovnaya, O., Bukanov, N.O., Donohue, L.C., Dackowski, W.R., Klinger, K.W. and Landes, G.M. (2000) Strong homophilic interactions of the Ig-like domains of polycystin-1, the protein product of an autosomal dominant polycystic kidney disease gene, PKD1. Hum. Mol. Genet. 9, 1641–1649.
[25] Wang, Y.K., Zhao, G.Y., Li, Y., Chen, X.L., Xie, B.B., Su, H.N. et al. (2010) Mechanistic insight into the function of the C-terminal PKD domain of the collagenolytic serine protease deseasin MCP-01 from deep sea *Pseudoalteromonas* sp. SM9913: binding of the PKD domain to collagen results in collagen swelling but does not unwind the collagen triple helix. J. Biol. Chem. 285, 14285–14291.
[26] Orikoshi, H., Nakayama, S., Hanato, C., Miyamoto, K. and Tsujibo, H. (2005) Role of the N-terminal polycystic kidney disease domain in chitin degradation by chitinase A from a marine bacterium, *Alteromonas* sp. strain O-7. J. Appl. Microbiol. 99, 551–557.
[27] Clapham, D.E. (2007) Calcium signaling. Cell 131, 1047–1058.
[28] Charlton, S., Moir, A.J., Baillie, L. and Moir, A. (1999) Characterization of the exosporium of *Bacillus cereus*. J. Appl. Microbiol. 87, 241–245.
[29] Chung, M.C., Popova, T.G., Millis, B.A., Mukherjee, D.V., Zhou, W., Liotta, L.A. et al. (2006) Secreted neutral metalloproteases of *Bacillus anthracis* as candidate pathogenic factors. J. Biol. Chem. 281, 31408–31418.
[30] Bogomolovas, J., Simon, B., Sattler, M. and Stier, G. (2009) Screening of fusion partners for high yield expression and purification of bioactive viscotoxins. Protein Expr. Purif. 64, 16–23.
[31] Lindmark, B., Rompikuntal, P.K., Vaitkevicius, K., Song, T., Mizunoe, Y., Uhlin, B.E. et al. (2009) Outer membrane vesicle-mediated release of cytolethal distending toxin (CDT) from *Campylobacter jejuni*. BMC Microbiol. 9, 220.
[32] Kabsch, W. (1993) Automatic processing of rotation diffraction data from crystals of initially unknown symmetry and cell constants. J. Appl. Crystallogr. 26, 795–800.
[33] Collaborative Computational Project, N (1994) The CCP4 suite: programs for protein crystallography. Acta Crystallogr. D 50, 760–763.
[34] Panjikar, S., Parthasarathy, V., Lamzin, V.S., Weiss, M.S. and Tucker, P.A. (2005) Auto-rickshaw: an automated crystal structure determination platform as an efficient tool for the validation of an X-ray diffraction experiment. Acta Crystallogr. D Biol. Crystallogr. 61, 449–457.
[35] Panjikar, S., Parthasarathy, V., Lamzin, V.S., Weiss, M.S. and Tucker, P.A. (2009) On the combination of molecular replacement and single-wavelength anomalous diffraction phasing for automated structure determination. Acta Crystallogr. D Biol. Crystallogr. 65, 1089–1097.
[36] Emsley, P. and Cowtan, K. (2004) Coot: model-building tools for molecular graphics. Acta Crystallogr. D Biol. Crystallogr. 60, 2126–2132.
[37] Emsley, P., Lohkamp, B., Scott, W.G. and Cowtan, K. (2010) Features and development of *Coot*. Acta Crystallogr. D Biol. Crystallogr. 66, 486–501.
[38] Murshudov, G.N., Vagin, A.A. and Dodson, E.J. (1997) Refinement of macromolecular structures by the maximum-likelihood method. Acta Crystallogr. D Biol. Crystallogr. 53, 240–255.
[39] Altschul, S.F., Gish, W., Miller, W., Myers, E.W. and Lipman, D.J. (1990) Basic local alignment search tool. J. Mol. Biol. 215, 403–410.